Organic Electronics 130 (2024) 107064

Contents lists available at ScienceDirect

Organic Electronics

journal homepage: www.elsevier.com/locate/orgel

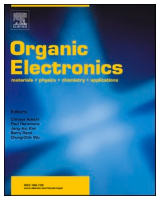

Synthesis and characterization of UV organic light-emitting electrochemical cells (OLECs) using phenanthrene fluorene derivatives for flexible applications

Sasikumar Arumugam [a,b], Yi Li [a], James E. Pearce [b,1], Katie L. Court [a], Edward H. Jackman [b], Oliver J. Ward [b], John Tudor [a], David C. Harrowven [b], Steve P. Beeby [a,*]

[a] Centre for Flexible Electronics and E-Textiles, School of Electronics and Computer Science, University of Southampton, Southampton, SO17 1BJ, UK
[b] School of Chemistry, University of Southampton, Southampton, SO17 1BJ, UK

ARTICLE INFO

Keywords:
UV emission
Organic light-emitting electrochemical cells
OLECs
Organic emitting molecules
UV emitting molecules
Printed electronics

ABSTRACT

This paper details how two new small molecules, based on phenanthrene, were developed, and tailored for light-emitting device applications. An account is provided of both the compound synthesis and the methodologies employed in device fabrication. The ink formulation was improved by the use of triflate counterions. Standard bottom emitting devices were constructed on ITO glass along with top emitting devices on a sputter coated silver on glass substrate. Both structures exhibit UV emissions from the synthesized molecules. Successful EL emission within the UV spectrum range has been achieved by spray coating these active molecules onto glass slides. The optimized solution-processed devices produce UV emission using a semi-transparent silver nanowire top electrode. This results in electroluminescence (EL) peaking at 398 nm, with a maximum EL emission intensity of 20.5 μW/cm^2.

1. Introduction

The production of light-emitting textiles is typically achieved by integrating emissive yarns into traditional textiles through standard weaving techniques [1]. However, this method is constrained by the available yarn designs and unsuitable patterns for weaving. As an alternative, off-the-shelf light-emitting diodes (LEDs) and electroluminescent (EL) strips can be stitched, adhered, or affixed to woven textiles. Nevertheless, these approaches necessitate manual assembly, making them unsuitable for large-scale production and better suited for customized, high-value applications. To address this limitation, flexible electroluminescent textiles have been developed using methods such as screen printing [2], slot die coating [3], inkjet printing [4], and dispenser printing [5]. These textiles incorporate thick inorganic emission layers but offer a limited range of colours for emission [4]. The high porosity and surface roughness of textiles generally hinder the precise fabrication needed for the deposition of LED functional layers, as each functional layer's thickness in an LED must fall within strict parameters.

Light-emitting electrochemical cells (LECs) offer a compelling alternative to explore in the realm of large-scale device designs, in addition to the extensively examined organic light-emitting diodes (OLEDs). What sets OLECs apart from OLEDs is their utilization of ionic components within the core light-emitting layer. A typical OLEC device is composed of a sole active layer that contains a blend of the active substance and ionic components, which is positioned between two electrodes [6–8]. The conduction of electronic charge in OLEC devices is facilitated by the mobility of ions, specifically salts, found within the active layer. This characteristic makes OLECs a more favourable option when compared to OLEDs which require additional functional layers. The active layers in OLEC devices can be created using cost-effective techniques such as solution-processing spin-coating or spray coating. Consequently, there has been a surge of research interest in developing efficient, budget-friendly OLECs [9]. Recent publications by Y. Choe and the Edman group at Umeå University have presented an economical and scalable approach for producing cost-effective solution processed OLEC devices on both glass and flexible substrates, respectively. Light-emitting materials within OLECs include ionic-transition metal complexes (iTMCs) or organic conjugated polymers [10–12].

* Corresponding author.
E-mail address: spb@ecs.soton.ac.uk (S.P. Beeby).
[1] Present address: School of Chemistry, University of Nottingham, Nottingham, UK, NG7 2RD.

https://doi.org/10.1016/j.orgel.2024.107064
Received 15 February 2024; Received in revised form 7 May 2024; Accepted 7 May 2024
Available online 8 May 2024

Iridium-based iTMCs have received significant attention due to their robust stability and higher photoluminescence efficiency in OLEC devices. Nevertheless, it's worth noting that the use of expensive and relatively rare rare-earth metals in these OLECs can lead to increased overall costs for large-scale applications [13].

In recent times, there has been a notable surge of interest in the utilization of organic conjugated polymers, such as the highly regarded super yellow polymer, as active materials in OLECs. These polymers are often combined with polyethylene oxide and inorganic salts. Notably, the authors have recently demonstrated the successful fabrication of OLECs on textile substrates, employing the super yellow polymer as the active layer [14]. While traditional substrates like rigid glass [15] are commonly used in OLEC device production, there's a growing trend towards incorporating plastics and textiles [11]. However, it's worth noting that the tri-component blends used for charge transport in OLECs can lead to phase separation in thin films [16]. To address this challenge, there is a rising interest in efficient emitters that also possess charge transport capabilities, making ionic organic small molecules highly desirable for playing dual roles in OLECs [17]. Recent successes have been observed in using charged organic small molecules as active materials that serve both as charge transport facilitators and emitters. Some notable studies, led by Choe et al. and others, have focused on small molecule OLECs for colour-emitting devices [10]. Within these studies, the conjugated units feature components like phenanthrene, carbazole, fluorene, phenothiazine, and imidazole derivatives, along with chemically integrated salt for ionic interactions [18].

The emission of ultraviolet (UV) light from OLECs is gaining attention due to the germicidal properties of UV light capable of destroying bacteria and viruses, known as ultraviolet germicidal irradiation (UVGI). The potential to print UV-emitting OLECs on textiles opens various applications, such as incorporating them into smart bandages for the treatment of infected wounds, thereby expediting the healing process. Additionally, UV emission from textiles can induce a change in colour through the photochromic effect [19]. Chen and colleagues have reported on their use of ionic 2,2-bifluorene in the creation of OLECs, incorporating methylimidazolium moieties as pendant groups [20]. This led to UV electroluminescent emission at 386 nm, with peak external quantum and power efficiencies of 0.15% and 1.06 mW/W, respectively. Poly (methyl methacrylate) (PMMA) was introduced into the active layer to enhance film quality and device performance. While PMMA did not play an active role, it effectively reduced leakage current and enhanced device efficiency. Nevertheless, challenges related to the poor solubility of the ionic molecule prompted an exploration of alternative molecule designs and synthesis. The authors had previously adapted Chen's work by modifying small molecule conjugated systems for Light-Emitting Electrochemical Cells, introducing octyl groups onto imidazole to enable the creation of spray-coated OLEC devices on glass substrates, which exhibited UV emissions of 1.29 μW/cm^2 for methyl imidazole and 0.89 μW/cm^2 for octyl imidazole [21].

In this research, we present the synthesis and characterization of ionic small molecules based on phenanthrene-fluorene-imidazole derivatives for the purpose of UV light-emitting electrochemical cells. In comparison to our prior work, we've replaced one of the fluorene components with a phenanthrene unit and introduced modifications to the imidazolium unit by incorporating methyl and octyl groups. These modifications were made to enable the creation of OLECs via solution processing techniques, specifically utilizing spray coating systems. The materials we synthesized were then employed in the fabrication of OLEC devices to assess their performance. The results obtained with phenanthrene derivatives reveal their capability to emit vibrant UV light and effectively serve as the active layer in single-component OLEC devices.

2. Experimental section

2.1. Materials

2,3,4,5,6-Pentafluorothiophenol (PFBT), acetone, acetonitrile, silver nanowires (AgNW), $CDCl_3$ and acetone-d_6 were purchased from Sigma Aldrich. 2-Bromofluorene, $B_2(pin)_2$, *N*-methylimidazole, *N*-octylimidazole, tetrabutylammonium bromide, $Pd(dppf)Cl_2$, $Pd(PPh_3)_4$, 1,6-dibromohexane, potassium acetate, 9-bromophenanthrene, and potassium trifluoromethanesulfonate were purchased from Fluorochem/Doug Discovery. Isopropanol, ethanol, methanol, diethyl ether, dichloromethane, dioxane, chloroform, hexane, ethyl acetate, petroleum ether, magnesium sulfate, conc. hydrochloric acid, potassium hydroxide, potassium carbonate, and toluene were purchased from Fisher Scientific. ITO glass was supplied by Kintec solutions. Encapsulation polymer was purchased from Norland optical adhesive NOA61. PEDOT: PSS was supplied by Heraeus. Silver target for sputtering was supplied by Labtech Ltd.

2.2. Molecules synthesis

2.2.1. General remarks

All air sensitive reactions were carried out under argon using flame dried apparatus. Reactions were monitored by TLC on Merck Silica Gel 60 Å F TLC plates and visualised with 254 nm UV followed by aqueous 1% $KMnO_4$ or CAMPH. Column chromatography was performed under slight positive pressure on Sigma Aldrich 40–63 μm 60 Å 230–400 Å silica. Reaction and chromatography solvents were removed using a rotary evaporator equipped with a diaphragm pump. Infrared spectroscopy was performed on a Nicolet iS5 Laboratory FT-IR spectrometer with spectra acquired on samples introduced by evaporation of $CDCl_3$ or $(CD_3)_2CO$ solutions. ^1H and ^{13}C NMR spectroscopy was performed on a Bruker AV400 (400/101 MHz) spectrometer at 298 K in $CDCl_3$ or acetone-d6. Chemical shifts are quoted as δ values in ppm using residual solvent peaks as the reference. Coupling constants *J* are given in Hz and multiplicity is described as follows: s, singlet; d, doublet; t, triplet; q, quartet; quin, quintet; m, multiplet; br, broad. HRMS data were obtained using a Bruker APEX III FT-ICR-MS with samples run in HPLC grade methanol. Electrospray mass spectrometry was performed on a directly injected Waters quadrupole MSD using ESI + ionisation with MeOH as solvent.

2.2.2. Synthetic procedures

2.2.2.1. 2-Bromo-9,9-bis-(6′-bromohexyl)fluorene, 2. The following procedures were adapted from that of Liu et al. [21]:

Gram scale: To a solution of 2-bromofluorene (**1**, 613 mg, 2.50 mmol), and TBAB (160 mg, 0.50 mmol) in KOH (50 mL, 50 wt% solution in water) was added 1,6-dibromohexane (4.00 mL, 26.0 mmol). The reaction mixture was heated to 75 °C for 18 h, then cooled to RT and diluted with CH_2Cl_2 (20 mL). The organic phase was separated, washed successively with water (2 × 15 mL), 2 M HCl (10 mL) and water (2 × 15 mL), dried over $MgSO_4$ and concentrated *in vacuo* to a pale-yellow oil. Purification by column chromatography (0–3% EtOAc in petroleum ether) afforded the *title compound* **2** as a pale-yellow oil (956 mg, 1.67 mmol, 67%).

Decagram scale: To a solution of 2-bromofluorene (**1**, 10.0 g, 41.0 mmol), and TBAB (1.59 g, 4.94 mmol) in KOH (200 mL, 50 wt% solution in water) was added 1,6-dibromohexane (65.0 mL, 422 mmol). The reaction mixture was heated to 75 °C for 17 h, then cooled to RT and diluted with CH_2Cl_2 (40 mL). The organic phase was separated, washed successively with water (50 mL), 2 M HCl (50 mL) and water (50 mL) then dried over $MgSO_4$ and concentrated *in vacuo* to a pale yellow oil. Purification by column chromatography (3 × 0–100% CH_2Cl_2 in hexane) afforded the *title compound* **2** as a pale yellow oil (18.3 g, 32.0

mmol, 78%). **IR** (film): ν_{max} 2930 (s), 2856 (m), 1729 (w), 1465 (m), 1442 (s), 1271 (m), 1062 (w), 823 (m), 776 (m), 738 (s) cm^{-1}. **^{1}H NMR** (400 MHz, $CDCl_3$): δ 7.68 (m, 1H, Ar**H**), 7.57 (dd, J = 7.2, 1.3 Hz, 1H, Ar**H**), 7.47 (dd, J = 7.6, 1.8 Hz, 1H, Ar**H**), 7.46 (s, 1H, Ar**H**), 7.38–7.30 (m, 3H, 3 × Ar**H**), 3.29 (t, J = 6.9 Hz, 4H, 2 × C**H$_2$**), 2.02–1.89 (m, 4H, 2 × C**H$_2$**), 1.67 (app. quin, J = 7.0 Hz, 4H, 2 × C**H$_2$**), 1.24–1.16 (m, 4H, 2 × C**H$_2$**), 1.13–1.03 (m, 4H, 2 × C**H$_2$**), 0.68–0.54 (m, 4H, 2 × C**H$_2$**) ppm. **^{13}C NMR** (100 MHz, $CDCl_3$): δ 152.6 (**C**), 149.9 (**C**), 140.2 (**C**), 140.0 (**C**), 130.0 (**CH**), 127.6 (**CH**), 127.1 (**CH**), 126.0 (**CH**), 122.8 (**CH**), 121.1 (**CH**), 121.0 (**C**), 119.8 (**CH**), 55.2 (**C**), 40.1 (2 × C**H$_2$**), 33.9 (2 × C**H$_2$**), 32.6 (2 × C**H$_2$**), 29.0 (2 × C**H$_2$**), 27.7 (2 × C**H$_2$**), 23.5 (2 × C**H$_2$**) ppm. **HRMS** (APPI): Found 567.9972, $C_{25}H_{31}Br_3$ $[M]^+$ requires 567.9970. Data consistent with literature values [21].

2.2.2.2. 2-[9,9-bis-(6-Bromohexyl)fluorenyl-4,4,5,5-tetramethyl[1.3.2] dioxaborolane, 3. The following procedure was adapted from that of Liu et al. [22]: A solution of fluorene **2** (5.80 g, 10.1 mmol), AcOK (5.05 g, 51.5 mmol) and $B_2(pin)_2$ (3.73 g, 14.7 mmol) in 1,4-dioxane (100 mL) was degassed by sonication under Ar for 10 min then $Pd(dppf)Cl_2$ (519 mg, 0.71 mmol) was added. Degassing was continued for a further 10 min then the solution was heated at 85 °C for 16 h. After cooling to RT, the reaction mixture was filtered, washed through celite with CH_2Cl_2 (150 mL), concentrated *in vacuo* to a black oil then partitioned between CH_2Cl_2 (50 mL) and water (50 mL). The organic phase was separated, washed with water (2 × 50 mL), dried over $MgSO_4$ and concentrated *in vacuo* to a dark brown oil. Purification by column chromatography (30–50% CH_2Cl_2 in petroleum ether) afford the *title compound* **3** as a pale yellow oil (5.46 g, 8.84 mmol, 87%) contaminated with a small quantity of pinacol. **IR** (film): ν_{max} 2977 (w), 2931 (m), 2857 (w), 1738 (w), 1609 (w), 1354 (s), 1144 (s), 743 (m) cm^{-1}. **^{1}H NMR** (400 MHz, $CDCl_3$): δ 7.82 (dd, J = 7.6, 1.0 Hz, 1H, Ar**H**), 7.76–7.69 (m, 3H, 3 × Ar**H**), 7.38–7.31 (m, 3H, 3 × Ar**H**), 3.27 (t, J = 6.8 Hz, 4H, 2 × C**H$_2$**), 2.07–1.92 (m, 4H, 2 × C**H$_2$**), 1.64 (app. quin, J = 7.2 Hz, 4H, 2 × C**H$_2$**), 1.40 (s, 12H, 4 × C**H$_3$**), 1.22–1.14 (m, 4H, 2 × C**H$_2$**), 1.10–1.01 (m, 4H, 2 × C**H$_2$**), 0.67–0.51 (m, 4H, 2 × C**H$_2$**) ppm. **^{13}C NMR** (100 MHz, $CDCl_3$): δ 150.9 (**C**), 149.5 (**C**), 144.1 (**C**), 140.9 (**C**), 133.8 (**CH**), 128.7 (**CH**), 127.6 (**CH**), 126.8 (**CH**), 122.8 (**CH**), 120.2 (**CH**), 119.0 (**CH**), 83.7 (2 × **C**), 54.9 (**C**), 40.1 (2 × C**H$_2$**), 33.9 (2 × C**H$_2$**), 32.6 (2 × C**H$_2$**), 29.0 (2 × C**H$_2$**), 27.7 (2 × C**H$_2$**), 25.0 (4 × C**H$_3$**), 23.4 (2 × C**H$_2$**) ppm. 1 × **C** not observed. **LRMS** (ESI^+): 621 ($[M + H (^{81}Br_2,^{11}B)]^+$, 100%), 620 ($[M + H (^{81}Br_2,^{10}B)]^+$, 58%), 619 ($[M + H (^{79}Br,^{81}Br,^{11}B)]^+$, 83%), 618 ($[M + H (^{79}Br,^{81}Br,^{10}B)]^+$, 18%), 617 ($[M + H (^{79}Br_2,^{11}B)]^+$, 4%), 616 ($[M + H (^{79}Br_2,^{10}B)]^+$, 26%). Data consistent with literature values [22].

2.2.2.3. 2-Phenanthrenyl-9,9-bis-(6′-bromohexyl)fluorene, 4. Dioxaborolane **3** (4.14 g, 6.69 mmol), tetrabutylammonium bromide (307 mg, 0.95 mmol), 9-bromophenanthrene (1.72 g, 6.70 mmol) and K_2CO_3 (4.64 g, 33.6 mmol) were partitioned between toluene (70 mL) and water (25 mL) then sonicated under argon for 15 min. $Pd(PPh_3)_4$ (281 mg, 0.24 mmol) was added and sonication was continued for a further 10 min. The mixture was heated at 85 °C for 15 h, cooled to RT, filtered through celite, washed sequentially with H_2O (2 x 30 mL), brine (30 mL), and H_2O (2 x 30 mL), dried over $MgSO_4$, and concentrated *in vacuo*. Purification by column chromatography (silica; 2%–5% EtOAc in hexane) gave the *title compound* as a colourless oil (327 mg, 0.46 mmol, 71%). **IR** (film): ν_{max} 2930 (m), 2856 (w), 1730 (m), 1545 (m), 1437 (s), 1364 (s), 1114 (s), 741 (s). **^{1}H NMR** (400 MHz, $CDCl_3$): δ 8.82 (1H, d, J = 8.2 Hz, Ar**H**), 8.76 (1H, d, J = 8.3 Hz, Ar**H**), 7.96 (2H, dd, J = 8.1, 1.2 Hz, Ar**H**), 7.86 (1H, dd, J = 7.7, 0.5 Hz, Ar**H**), 7.82–7.77 (2H, m, Ar**H**), 7.73–7.62 (3H, m, Ar**H**), 7.59–7.53 (2H, m, Ar**H**), 7.52 (1H, dd, J = 1.5, 0.5 Hz, Ar–**H**), 7.43–7.34 (3H, m, Ar**H**), 3.30 (4H, t, J = 6.8 Hz, C**H$_2$**Br), 2.03 (4H, t, J = 8.3 Hz, C**H$_2$**), 1.70 (4H, quin, J = 7.1 Hz, C**H$_2$**), 1.31–1.21 (4H, m, C**H$_2$**), 1.18–1.08 (4H, m, C**H$_2$**), 0.91–0.68 (4H, m, C**H$_2$**) ppm. **^{13}C NMR** (101 MHz, $CDCl_3$): δ (100 MHz, $CDCl_3$) 150.6 (**C**), 150.4 (**C**), 140.9 (**C**), 140.4 (**C**), 139. 6 (**C**), 139.1 (**C**), 131.6 (**C**), 131.3 (**C**), 130.7 (**C**), 129.9 (**C**), 128.8 (**C**), 128.6 (**C**), 127.4 (**C**), 127.2 (**C**), 127.0 (**C**), 126.90 (**C**), 126.85 (**C**), 126.6 (**C**), 126.5 (2 x **C**), 124.6 (**C**), 123.0 (**C**), 122.8 (**C**), 122.6 (**C**), 119.9 (**C**), 119.6 (**C**), 55.0 (Ar_2**C**), 40.2 (2 x **C**H_2), 33.9 (2 x **C**H_2Br), 32.6 (2 x **C**H_2), 29.1 (2 x **C**H_2), 27.8 (2 x **C**H_2), 23.7 (2 x **C**H_2) ppm. **HRMS** (APPI): Found 666.1498, $C_{39}H_{40}Br_2$ $[M^+$ ($^{79}Br_2$)] requires 666.1497.

2.2.2.4. 9,9-bis-[6-(3-Methylimidazol-3-ium-1-yl)hexyl]-2-(phenanthren-9-yl)-fluorene triflate, 5a. A solution of dibromide **4** (817 mg, 1.2 mmol) and *N*-methylimidazole (0.24 mL, 3.0 mmol) in toluene (10 mL) was heated at 100 °C for 20 h, then cooled to RT. The solvent was decanted away from the resulting gum, then the gum was dissolved in methanol (5 mL) and an aqueous solution of CF_3SO_3K (0.1 M, 30 mL) was added over 10 min. The aqueous phase was decanted away from the resulting gum, then the gum was triturated with diethyl ether (100 mL) and subjected to sonication under water for 1 h. The aqueous phase was decanted away from the resulting gum and acetone (100 mL) was added. Concentration *in vacuo* afforded the *title compound* **5a** (745 mg, 0.77 mmol, 63%) as an off-white gum. **IR** (film): ν_{max} 2929 (w), 2858 (w), 1455 (w), 1252 (vs), 1159 (s), 1030 (vs), 764 (m), 638 (vs), 576 (m). **^{1}H NMR** (400 MHz, acetone-d_6): δ 9.00–8.86 (4H, m, Ar**H**), 8.06 (1H, dd, J = 7.8, 1.3 Hz, Ar**H**), 7.99 (1H, d, J = 7.7 Hz, Ar**H**), 7.91–7.87 (1H, m, Ar**H**), 7.85–7.80 (2H, m, 2 × Ar**H**), 7.77–7.67 (3H, m, Ar**H**), 7.64 (4H, app. t, J = 1.8 Hz, 2 × Ar**H**), 7.61 (4H, app. t, J = 1.8 Hz, 2 × Ar**H**), 7.57 (1H, d, J = 1.1 Hz, Ar**H**), 7.55–7.46 (3H, m, 3 × Ar**H**), 7.41–7.33 (2H, m, 2 × Ar**H**), 4.02 (4H, t, J = 7.1 Hz, 2 × C**H$_2$**N), 3.78 (6H, s, 2 × C**H$_3$**), 2.06–1.95 (4H, m, 2 × C**H$_2$**), 1.59 (4H, quin, J = 7.3 Hz, 2 × C**H$_2$**), 1.13–0.96 (8H, m, 4 × C**H$_2$**), 0.73–0.53 (4H, m, 2 × C**H$_2$**) ppm. **^{13}C NMR** (101 MHz, acetone-d_6): 150.3 (**C**), 150.1 (**C**), 140.3 (**C**), 140.0 (**C**), 138.8 (**C**), 138.4 (**C**), 136.4 (**C**), 131.1 (**C**), 130.6 (**C**), 130.3 (**C**), 129.4 (**C**), 128.7 (**C**), 127.4 (**C**), 127.2 (**C**), 127.1 (**C**), 127.0 (**C**), 126.8 (**C**), 126.7 (**C**), 126.1 (**C**), 125.5 (**C**), 124.5 (**C**), 123.5 (**C**), 122.9 (**C**), 122.8 (**C**), 122.3 (**C**), 122.2 (**C**), 120.1 (**C**), 119.1 (**C**), 115.9 (**C**), 54.7 (**C**), 48.7 (**C**H_3), 35.7 (**C**H_2), 30.7 (**C**H_2), 29.4 (**C**H_2), 28.9 (**C**H_2), 25.4 (**C**H_2), 23.6 (**C**H_2) ppm. **HRMS** (ESI+): Found 366.2091 $[M]^{2+}$, $C_{47}H_{52}N_4^{2+}$ requires 366.2091.

2.2.2.5. 9,9-bis-[6-(3-Octylimidazol-3-ium-1-yl)hexyl]-2-(phenanthren-9-yl)-fluorene triflate, 5b. A solution of dibromide **4** (434 mg, 0.65 mmol) and *N*-octylimidazole (0.27 mL, 1.34 mmol) in toluene (5.0 mL) was heated at 100 °C for 24 h, then cooled to RT. The solvent was decanted away from the resulting gum, then the gum was dissolved in methanol (5 mL) and an aqueous solution of CF3SO3K (1 M, 10 mL) was added over 10 min. The aqueous phase was decanted away from the resulting gum, then the gum was triturated with diethyl ether (100 mL) and subjected to sonication under water for 1 h. The aqueous phase was decanted away from the resulting gum and acetone (100 mL) was added. Concentration *in vacuo* afforded the title compound **5b** (590 mg, 0.51 mmol, 78%) as an off-white gum. **IR** (film): ν_{max} 2930 (w), 1242 (vs), 1228 (vs), 1170 (s), 1025 (vs), 636 (vs). **^{1}H NMR** (400 MHz, acetone-d_6): δ 9.09 (2H, t, J = 1.5 Hz, Ar–**H**), 8.95 (1H, d, J = 8.2 Hz, Ar–**H**), 8.88 (1H, d, J = 8.6 Hz, Ar–**H**), 8.02 (1H, dd, J = 1.6, 7.7 Hz, Ar–**H**), 7.99 (1H, dd, J = 0.5, 7.7 Hz, Ar–**H**), 7.95–7.88 (2H, m, Ar–**H**), 7.81 (1H, s, Ar–**H**), 7.77–7.65 (7H, m, Ar–**H**), 7.62–7.48 (4H, m, Ar–**H**), 7.44–7.35 (2H, m, Ar–**H**), 4.32–4.18 (8H, m, C**H$_2$**), 2.17–2.07 (4H, m, C**H$_2$**) 1.93–1.83 (4H, m, C**H$_2$**), 1.77 (4H, quin, J = 7.2 Hz, C**H$_2$**), 1.32–1.11 (28H, m, C**H$_2$**), 0.90–0.81 (6H, t, J = 6.85 Hz, C**H$_3$**), 0.90–0.62 (4H, m, C**H$_2$**). **^{13}C NMR** (101 MHz, acetone-d_6): δ 151.0 (**C**), 150.8 (**C**), 141.2 (**C**), 140.9 (**C**), 139.8 (**C**), 139.3 (**C**), 136.3 (**CH**), 132.0 (**C**), 131.5(**C**), 131.2 (**C**), 130.3 (**C**), 129.1 (**CH**), 129.1 (**CH**), 127.7 (**CH**), 127.6 (**CH**), 127.4 (**CH**), 127.2 (**CH**), 127.1 (**CH**), 127.0 (**CH**), 126.9 (**CH**), 125.0 (**CH**), 123.6 (**C**), 123.4 (**CH**), 123.2 (**CH**), 123.0 (**CH**), 123.0 (**CH**), 122.9 (**CH**), 120.2 (**CH**), 120.2 (**CH**), 120.0 (**C**), 55.4 (**C**), 49.9 (**C**H_2), 49.8 (**C**H_2), 40.1 (**C**H_2), 31.9 (**C**H_2), 30.1 (**C**H_2), 30.1 (**C**H_2), 29.4 (**C**H_2), 29.2 (**C**H_2), 29.0 (**C**H_2), 26.2 (**C**H_2), 26.0 (**C**H_2), 24.0 (**C**H_2), 22.7 (**C**H_2), 13.8 (**C**H_3) ppm. **HRMS**

(ESI+): Found 434.3197 $[M]^{2+}$, $C_{61}H_{80}N_4^{2+}$ requires 434.3186.

3. Fabrication and characterisation

3.1. Bottom emitting UV-OLECs on ITO glass substrate

The ITO glass slides were rinsed with deionized water and acetone followed by UV ozone treatment in sequence to remove any surface contamination prior to functional coating. Fig. 1a and b shows both the isometric diagram of the OLEC standard bottom emitting structure along with the top emitting inverted device structure used in this research. A PEDOT: PSS suspension in water was first spin coated directly on the ITO patterned substrate and annealed on a hotplate at 120 °C for 20 min in a The UV emitting active layer **5a** was spin coated in an ambient environment. Molecule **5a** was dissolved in acetonitrile at a concentration of 1g dissolved in 5 mL of acetonitrile. Annealing of the spin coated **5a** layer was undertaken at 70 °C for 5 h in a nitrogen filled box oven. To complete UV OLEC fabrication, a silver top electrode was sputter coated through a pre-defined shadow mask, by a coating current of 70 mA to achieve a thickness of 100 nm. The top electrode mask was pre-defined to achieve three light emitting pixels (active area of the electrode, 2 mm^2). Silver conductive paint was subsequently applied to establish contact points for testing. Finally, the devices were encapsulated by drop casting an epoxy formulation onto the surface and covering with a coverslip. The fully encapsulation system was then UV cured with a 365 nm wavelength mercury lamp. The encapsulation process happened inside the Argon filled glove box to avoid oxygen being trapped in the devices. Spray coating layers of **5a** and **5b** was also attempted under atmospheric conditions with a nitrogen (N_2) carrier gas in pneumatic spray coating system. The distance from the nozzle to the substrate was 15 cm with a differential inlet/outlet pressure of 0.3 bar. Attempts to fabricate a spray coated layer of **5a** onto the PEDOT:PSS coated ITO were unsuccessful as no uniform layer of **5a** could be achieved. It was possible however, to achieve a uniform spray coated layer of the **5b** compound (see Fig. 4b) and hence to complete the fabrication of the devices. Molecule **5b** was dissolved at a concentration of 1 g in 0.5 mL of ethanol and its high solubility led to greatly improved processing capability for spray coating.

3.2. Top emitting UV-OLECs on glass substrates

Silver electrodes were sputter coated on glass substrates at the rate of 1 nm per 30 s to achieve a thickness of 100 nm. As sputtered silver has a low surface energy, a self-assembled monolayer treatment (SAM) was dip coated onto the surface to alter the energy level of the silver and enable the wetting of the subsequent functional layers. This was carried out by immersing the silver electrodes on glass into the 2 μl of PFBT (Penta fluorobenzene thiol) in 1 mL of Isopropanol solution for 20 min. The SAM modified silver electrodes were then used to fabricated devices for the functional layers. Molecule **5b** in ethanol was spray coated on the silver electrodes and annealed at 70 °C for 5 h in a nitrogen filled box oven. After this, a PEDOT:PSS suspension in water was spray coated directly on the active layer and again annealed at 120 °C for 20 min in a conventional box oven. Finally, a semi-transparent silver nanowire (AgNW) electrode was spray coated to form top electrodes using pre-defined mask and annealed at 60 °C. The devices were completed and encapsulated using the same method as that employed for the ITO glass substrates.

3.3. Characterisation methods

The following instrumentation were utilized: Phenom G6 ProX Scanning Electron Microscope (SEM) system was employed to capture cross-sectional SEM images of the UV OLEC devices to assess the thickness of the functional layers. Ultraviolet–visible (UV–Vis) transmission and absorption measurements were conducted using a DS5 Dual Beam UV–Vis Spectrophotometer, supplied by Edinburgh Instruments. To deposit the top electrode, a high-speed sputter coater machine (Safematic CCU 010) was utilized. The UV emission intensity and spectrum of the OLECs were measured with a UV/Vis/NIR spectroradiometer (Stellar-RAD 250–1100 nm). A Thorlabs-supplied 340 nm laser (M340L4) with a power output of 53 mW (minimum) and 700 mA served as the excitation source for photoluminescence (PL) emission. An adjustable Collimation Adapter (SM2F32-A) featuring a Ø2″ Lens with AR Coating and a wavelength range of 350 nm–700 nm was used in conjunction with the 340 nm laser source for PL measurements. For EL spectrum determination, UV OLEC devices fabricated on ITO pre-coated glass slide substrates were measured in a bottom-emission configuration. Absorption and PL measurements were conducted on both solution-state samples using a cuvette and on spray-coated films. In the case of the coated film on a glass substrate, the UV emitting film possessed a thickness of 250 nm. The material's absorption peak defined the wavelength range required for the PL measurement. PL excitation occurred within this range, but wavelengths below the absorption peak also induced PL emission.

4. Results and discussion

Syntheses of the active fluorene-phenanthrene systems **5a** and **5b** from commercially available 2,7-dibromo-9*H*-fluorene **1** were accomplished using the four-step sequence outlined in Scheme 1. Thus, *bis*-bromide **2** could be prepared on a decagram scale in 78% yield by alkylation of **1** using KOH and 10 equiv. 1,6-dibromohexane. A Suzuki-Miyaura cross coupling sequence then introduced the phenanthrene moiety (**2** → **3** → **4**), allowing the targets to be prepared by treatment with *N*-methyl- or *N*-octyl-imidazole, respectively, and ion exchange with potassium triflate.

4.1. Absorption and photoluminescence measurements

The photophysical characteristics of molecules **5a** and **5b** were investigated with both UV–Vis and PL spectrometers. Fig. 2 presents the absorption spectra of these compounds in acetonitrile. These spectra exhibit absorption peaks at 210 nm, 253 nm, and 309 nm for **5a** and very

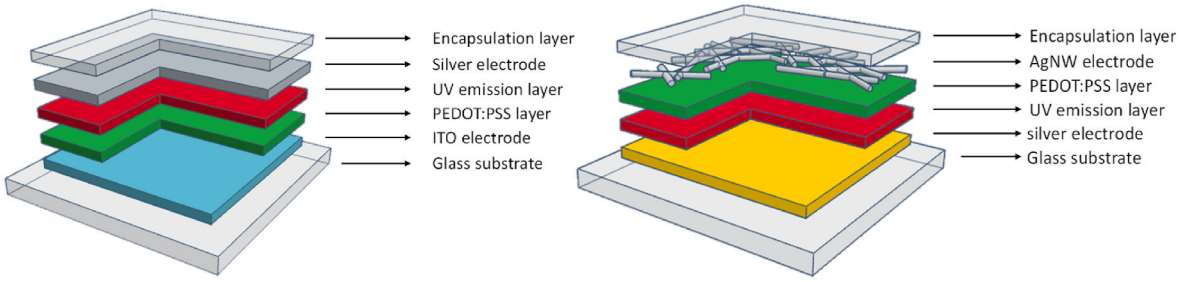

Fig. 1. (a) Schematic drawing of spray coated UV light emission through an ITO electrode and (b) a UV light top emission device fabricated on a self-assembled monolayer (SAM) treated silver glass substrates.

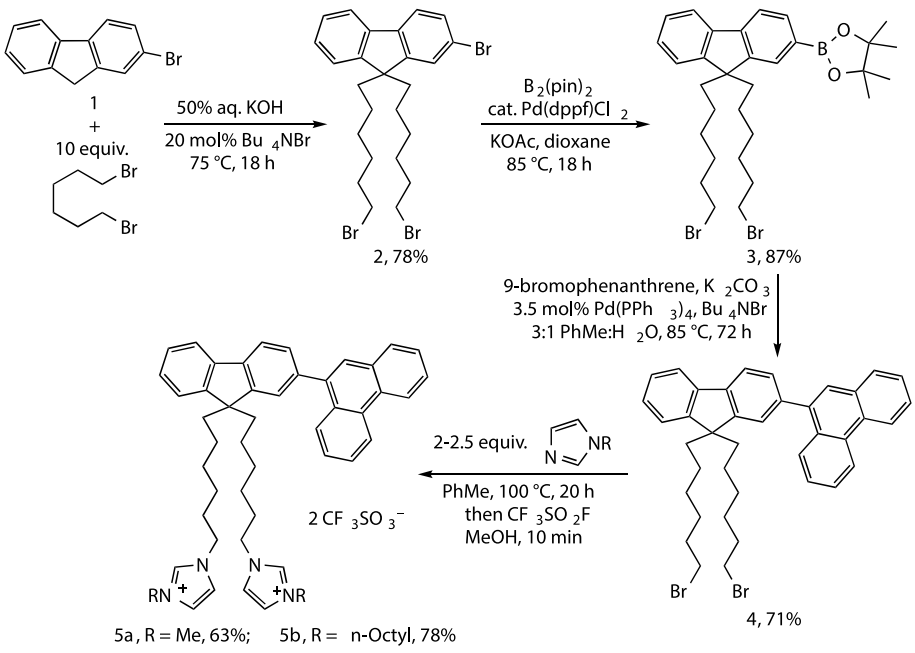

Scheme 1. Synthesis of the active fluorene-phenanthrene systems **5a** and **5b**.

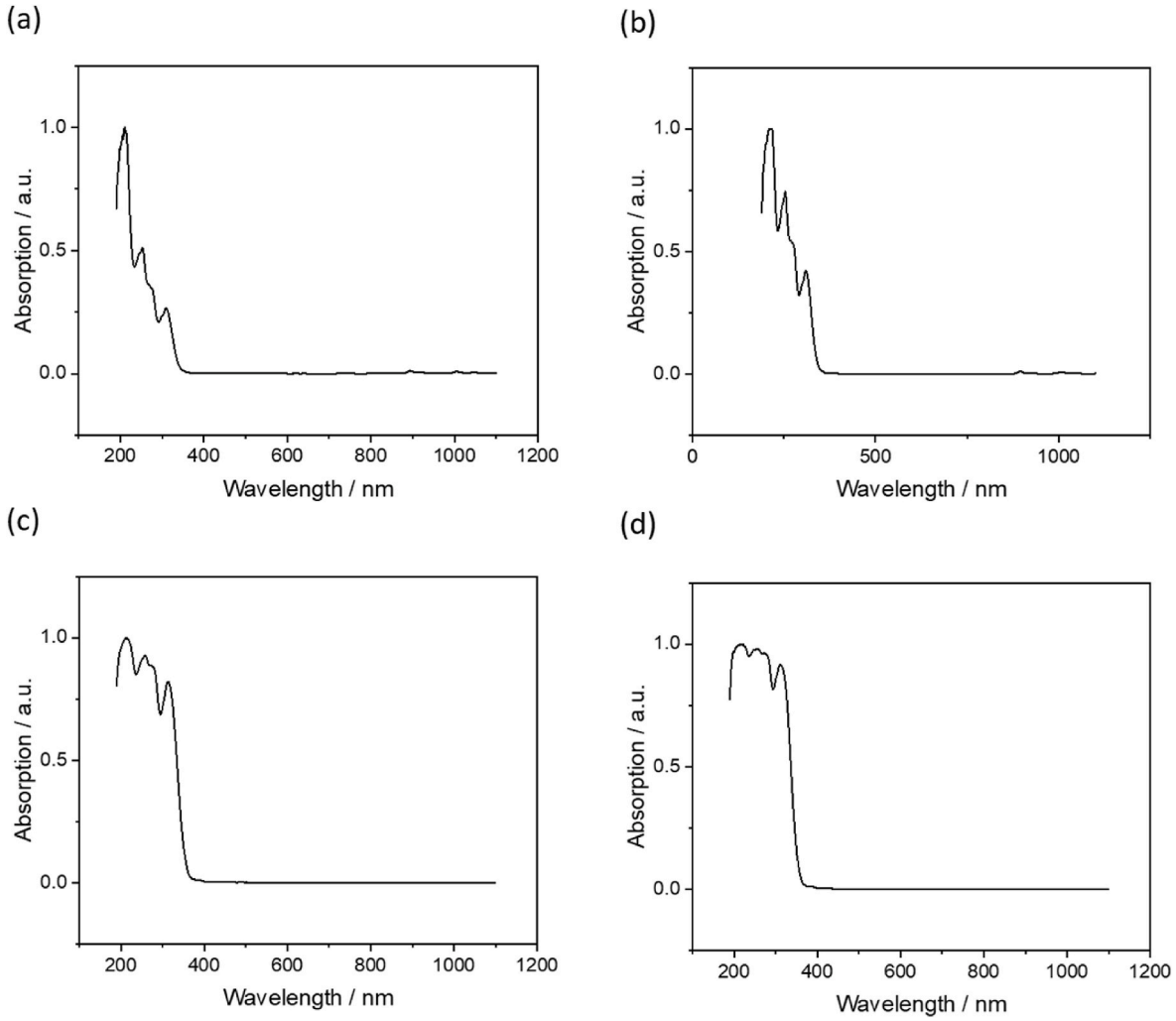

Fig. 2. Absorption measurement for solution (a) UV emitters **5a** (b) **5b** and thin film state for UV emitters (c) **5a** and (d) **5b**.

similar peaks at 214, 253 and 310 nm for **5b**. These peaks correspond to π-π* transitions. From these absorption features, the energy gap (Eg) was determined to be 3.23 and 3.24 eV for **5a** and **5b**, respectively. Furthermore, thin film absorption spectra displayed a slight broadening of the curves, with maxima at 214, 258 and 313 nm for **5a**, and 216, 257 and 311 nm for **5b**. This broadening can be attributed to intermolecular interactions in the thin film state. Both compounds were excited at an available 340 nm laser diode, leading to emission peaks at 397 and 510 nm for **5a** and 400, and 510 nm for **5b** in acetonitrile solution, as shown in Fig. 3. In the case of annealed thin films, emissions for both **5a** and **5b** were observed at 344, 413, and 490 nm and 371, 405, and 521 nm, respectively. Notably, **5b** exhibited a red shift of approximately 30 nm in the thin film state compared to its solution PL emission, which can be attributed to the close packing of molecules in the amorphous thin film or solvent interactions.

4.2. SEM characterisation

To further investigate the impact of small molecules combined with ionic additives on the performance of light emission, we conducted a characterization of the thin films using scanning electron microscopy (SEM), as depicted in Fig. 4. The SEM image of the spin coated **5a** film reveals a low surface coverage and a considerable density of pinholes, which appears to be the primary cause of short-circuits and instability in device performance. The surface coverage of the **5b** film was notably improved, and the spray coated film exhibited a more compact structure, as shown in Fig. 4b. Additionally, the **5b** film displayed fewer voids and holes among its grains, indicating a uniform film morphology and excellent coverage.

The sandwich structure of the device (Fig. 4a) allows for the clear distinction of each functional layer, and the roughly measured thicknesses of PEDOT:PSS, active layer, and silver layer are 100 nm, 600 nm, and 100 nm, respectively. While the thickness of the spray-coated OLEC active layer is similar to the emitting layer in a typical polymer OLEC, it may not be the ideal thickness for OLEC devices in this study. Thickness variations ranging from 300 nm to 1 μm were therefore tested, and the results revealed high leakage current in devices with 1 μm thick active layers. The optimal thickness for OLEC devices was found to be in the range of 500 nm–700 nm, with illumination occurring at a turn-on voltage of 3V, gradually increasing from 1 V.

4.3. Electrical and luminescent measurement

4.3.1. Molecules 5a and 5b

For device measurement, molecule **5a** was denoted as Device 1 and molecule **5b** as Device 2, both on ITO glass. Device 1 emitted UV light at 394 nm, while Device 2 emitted at 398 nm. To enhance device stability, we selected driving voltages near the energy gaps of **5a** and **5b** (3.56 eV in solution). The energy gaps in films are typically smaller than those in solution due to environmental polarization, allowing OLEC devices to be activated at bias voltages as low as 3V. These **5a** and **5b** OLEC devices displayed similar electrical characteristics. Devices 1 and 2 are activated on at 3 V. The maximum UV brightness was achieved at 8 V for Device 1 V and 5 V for Device 2. After voltage application, both brightness and

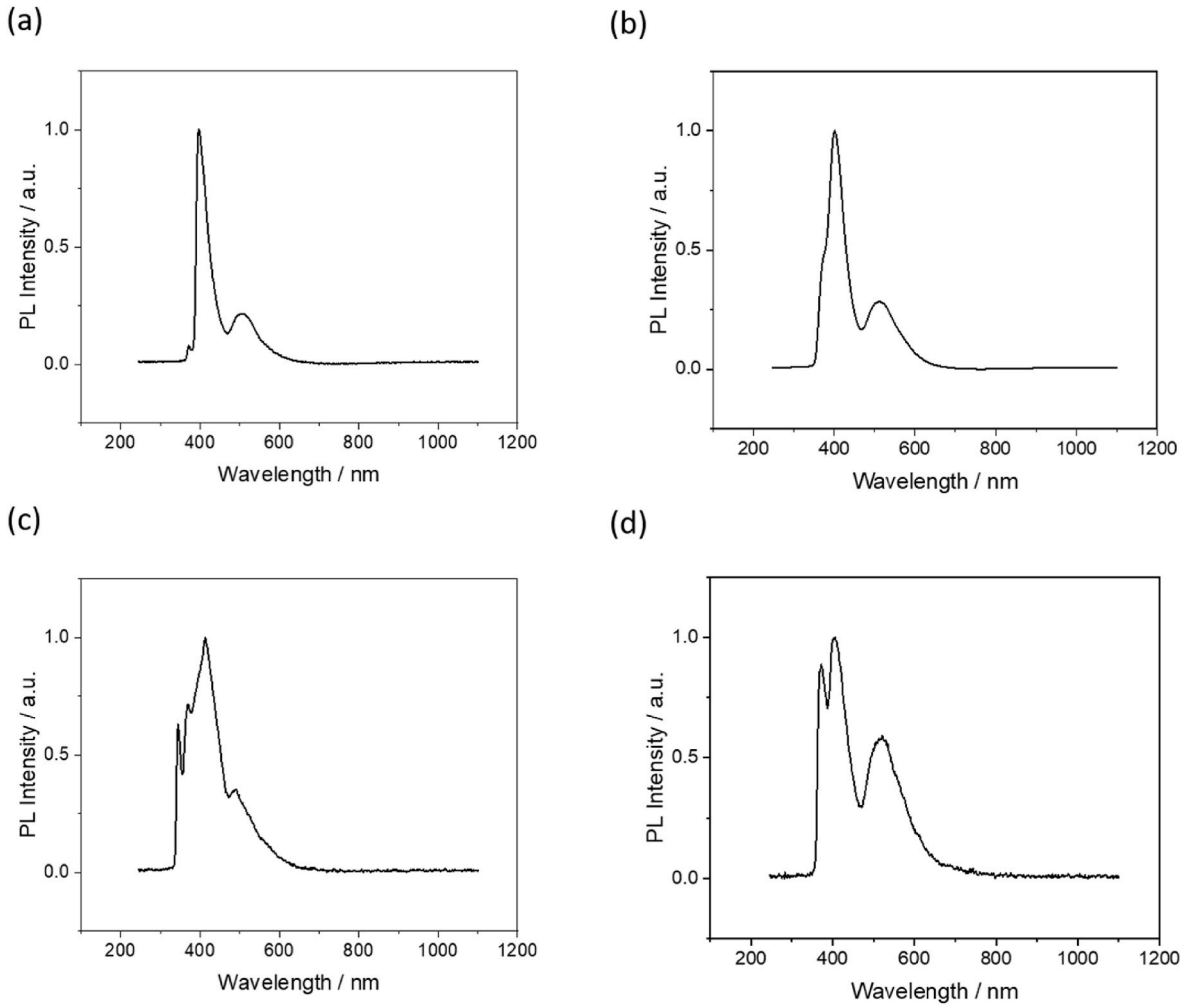

Fig. 3. Photoluminescent (PL) measurement for solution (a) UV emitters **5a** and (b) **5b**, and thin film state for UV emitters (c) **5a** and (d) **5b**.

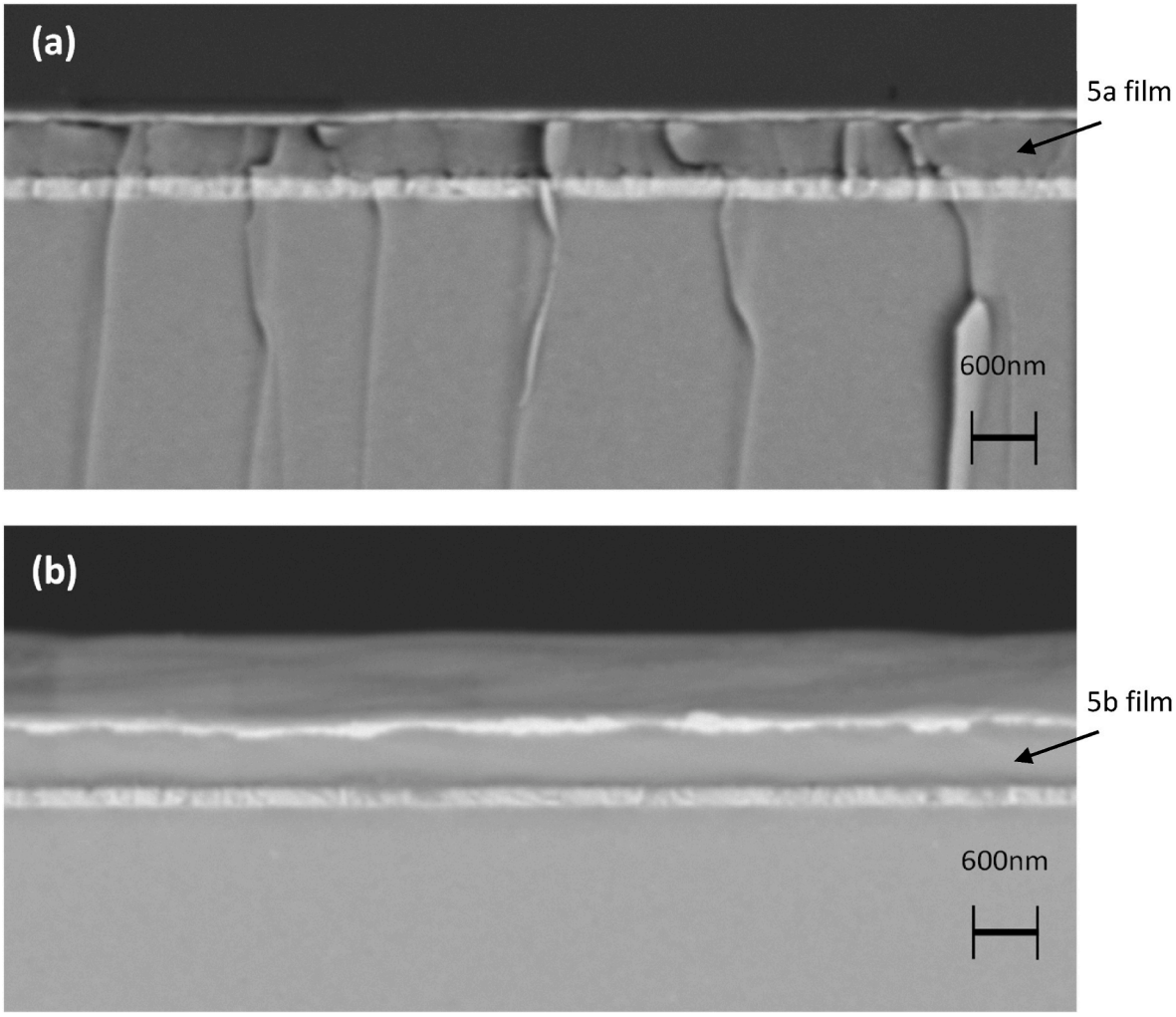

Fig. 4. cross sectional view SEM images of spray coated UV OLECs (a) on ITO glass substrate, bottom to top, 120 nm thick ITO layer, spin coated 100 nm PEDOT:PSS layer, spin coated 600 nm thick UV emission layer **5a**, sputtered 100 nm thick silver top electrode; (b) on ITO glass substrate, bottom to top, 120 nm thick ITO layer, spin coated 100 nm PEDOT:PSS layer, spray coated 600 nm thick UV emission layer **5b**, sputtered 100 nm thick silver top electrode (the surface of the device is also visible in **4b** due to the slight angle of the substrate).

device current initially increased over time, reaching peak UV output before gradually declining. The time to reach maximum UV brightness decreased as the bias voltage swept from 3 V to 12 V, likely due to a higher accumulation rate of mobile ions, facilitating the formation of doped regions near the electrode under a 12 V electric field.

Under the same bias voltage sweep, Device 2 reached its maximum brightness at 5V more quickly than Device 1, indicating a faster ion accumulation rate, leading to faster doped region formation. This is attributed to the better interface between the spray-coated functional layers and a lack of charge injection barriers. The gradual decrease in brightness and current density over time after reaching peak values in encapsulated devices is linked to the degradation of the emissive material during OLEC operation. The 20.5 $\mu W/cm^2$ maximum brightness and 215 mA/cm^2 current density as shown in Table 1 achieved in fresh devices for **5b** could not be fully recovered in subsequent measurements, even under the same operating conditions. Fig. 5 illustrates I/V curve and EL spectrum for **5a** and **5b** UV emitters. Table 2 shows the device architecture of all three devices and device emission and their application methods utilized in the research.

We assessed the duration of each device's lifespan by determining the time it took for it to degrade from its peak UV brightness to the point of failure. As an illustration, the lifespan of Device 1 decreased from 10 min (with a bias voltage increase from 3 V to 8 V) to 1 min (under a consistent bias of 7V). Conversely, Device 2's lifetime decreased from 20 min to 1 min during 3 V–5 V voltage increase and at 5 V respectively. Higher bias voltage accelerated irreversible multiple oxidation and subsequent decomposition of the UV emission material, leading to the degradation of the OLEC devices. Despite the shorter lifetimes observed, the OLEC performance is promising, and further modifications to the molecule could enhance UV emission longevity.

Table 1
collection of electroluminescent data of UV OLEC devices 1, 2 and 3.

Devices	EL Peak (nm)	V_{on} (V)	V_{max} (V)	Jmax (mA/cm^2)	Lmax ($\mu W/cm^2$)	Lifetime (min)
1	394	3	8	190	14.52	<1
2	398	3	5	215	20.57	<1
3	410	2.5	10	195	6.28	<1

4.3.2. Molecule 5b

To further assess the smart ink's performance, an inverted device structure was created on glass substrates with a layer of silver as the bottom electrode. This structure enables top emission and is compatible with solution-processing devices. Fig. 6 shows the SEM image of the inverted OLEC structure, with silver used as the bottom electrode and AgNW employed as the top transparent electrode. The device

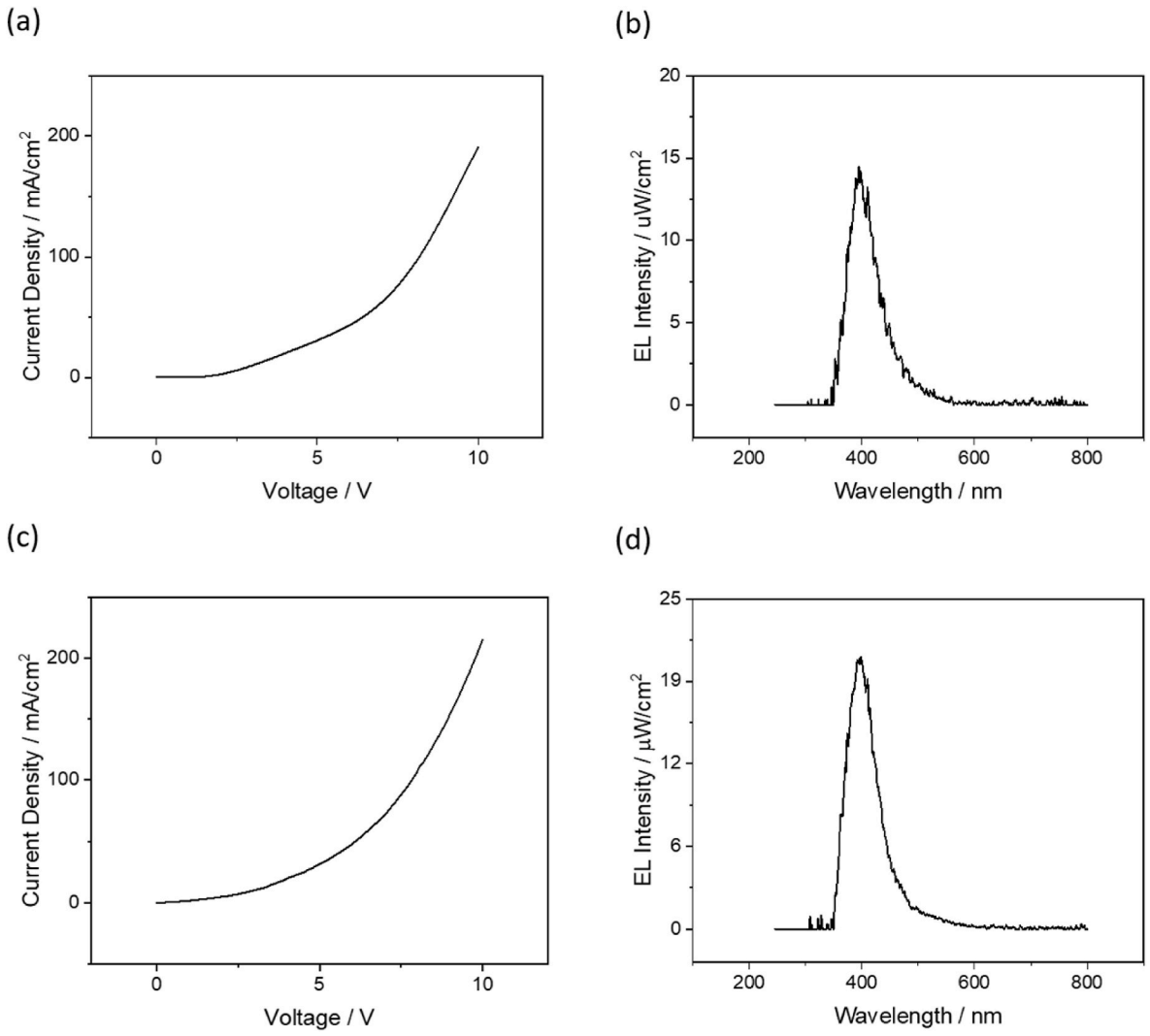

Fig. 5. Current and Voltage sweep (I/V) curve for UV emitters (a) **5a** and (c) **5b**, on ITO glass substrates. Electroluminescent (EL) spectrum of spray coated OLECs on pre-coated ITO glass slides with (b) **5a** (d) **5b**.

Table 2
Table shows the device architecture, emission, and their application methods.

Devices	Device Architecture	Emission	Deposition
1	Glass/ITO/PEDOT:PSS/molecule **5a**/ Silver	Bottom Emitting	Spin Coating
2	Glass/ITO/PEDOT:PSS/molecule **5b**/ Silver	Bottom Emitting	Spray Coating
3	Glass/silver/molecule **5b**/PEDOT: PSS/AgNW	Top Emitting	Spray Coating

configuration follows this sequence: glass/Silver/Active layer/PEDOT: PSS/AgNW. Initial attempts to spray coat the active layer directly onto thermally sputtered silver substrates were unsuccessful in achieving a uniform functional active layer due to the low surface energy of the silver electrodes. To address this, the SAM approach was applied to the silver electrodes to achieve a uniform active layer using the spray coating method. The direct spraying of AgNW onto the active layer was found to significantly dissolve the active layer's constituents. It was also observed that a highly conductive, pinhole-free, and non-porous uniform layer is crucial for an effective light-emitting transparent electrode. For these reasons, an aqueous PEDOT:PSS suspension was chosen for spray coating to protect the active layer, followed by the application of the AgNW transparent electrode. Before analysing the OLEC's performance, the device was encapsulated. The SEM image presents a cross-sectional view of the optimized top-emission device, depicting all the distinct and uniform functional layers. The average thickness of **5b** active layer is 650 ± 50 nm, and the HTL thickness is approximately 250 nm. The functional layer interfaces between the SAM-treated silver electrode and PEDOT: PSS are exceptionally smooth, devoid of any visible voids or interface imperfections. This continuous morphology, achieved through spray coating under ambient air conditions, is vital for ensuring the device's high performance.

Fig. 7 illustrates the I/V and EL for device 3, using molecule **5b**. The luminance and current density of the top-emission devices gradually increased with rising voltage, reaching a luminance of 6.28 µW/cm^2 and a current density of 195 mA/cm^2 for device 3. While the turn-on voltage is 2.5 V, the maximum brightness was achieved at 10 V, as it is higher compared to device 2. This is due to the scaffold-like nature of the transparent AgNW, which requires a higher bias voltage to fully illuminate the top electrode rather than shining through the micro-holes of the top electrode. The inverted structure means the light is emitted from the top surface of the OLECs and this is essential for the textile substrate which does not allow bottom emission. The key challenge is to use solution processing to deposit suitable patterned transparent/translucent top electrodes that enable the top emission.

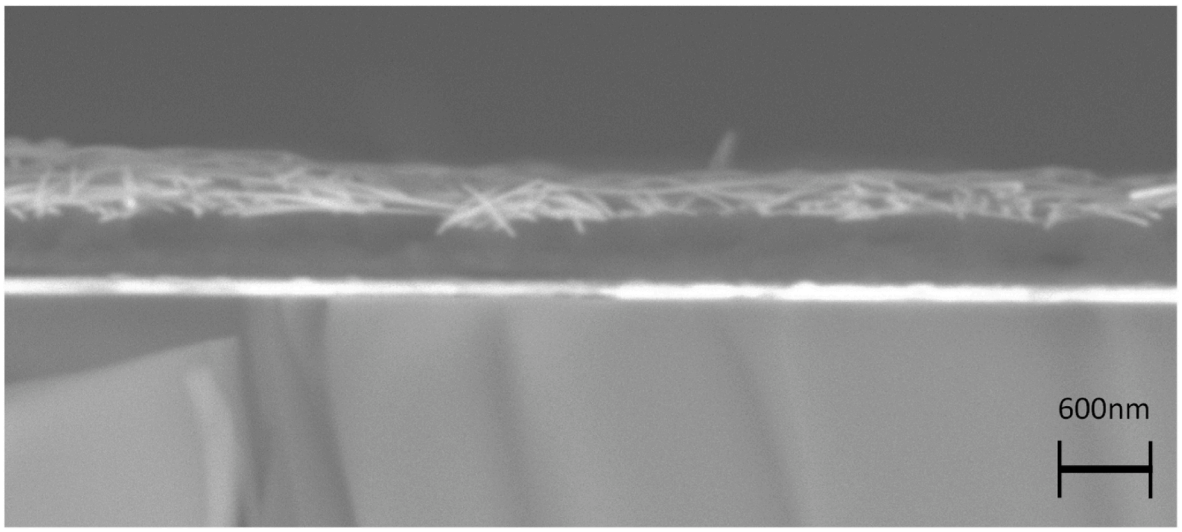

Fig. 6. Cross sectional view SEM images of spray coated UV OLECs on silver glass substrate, top to bottom: silver nanowires 100 nm, PEDOT:PSS 50 nm, **5b** emission layer 600 nm, SAM treated sputtered silver 100 nm.

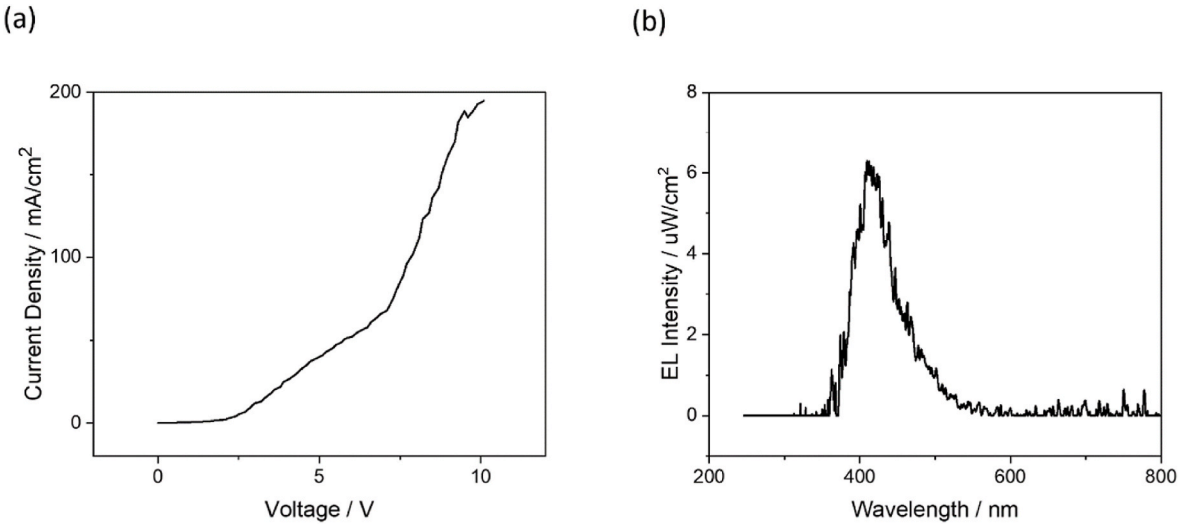

Fig. 7. Current and Voltage sweep (I/V) curve for UV emitters.

5. Conclusions

In this study, we successfully synthesized two organic materials capable of emitting UV light. These materials feature fluorene-phenanthrene segments and were synthesized in high yield. Notably, the synthesized compounds demonstrated remarkable UV light emission, with wavelengths of 394 nm for compound **5a** and 398 nm for compound **5b**. To impart the crucial ionic properties necessary for OLECs, we chemically attached methyl and octyl imidazolium groups as pendant units to the hexyl chains. Notably, the enhanced solubility observed with the octyl analogue **5b** proved critical for the creation of uniform spray-coated thin films without aggregation or pinholes. OLEC devices were fabricated with both bottom and top emission using the active material, resulting in strong UV PL and EL emissions. The UV OLECs constructed exhibited peak electroluminescent intensity values ranging from 14.52, 20.57, 6.28 μW/cm^2 for devices 1, 2, and 3 respectively. These findings hold significant importance as they are a crucial step towards the development of energy-efficient full-colour displays and solid-state lighting.

CRediT authorship contribution statement

Sasikumar Arumugam: Writing – original draft, Methodology, Investigation, Formal analysis. **Yi Li:** Writing – original draft, Validation, Investigation, Formal analysis. **James E. Pearce:** Methodology, Investigation, Formal analysis. **Katie L. Court:** Writing – review & editing, Methodology, Investigation, Formal analysis. **Edward H. Jackman:** Methodology, Investigation, Formal analysis. **Oliver J. Ward:** Methodology, Investigation, Formal analysis. **John Tudor:** Writing – review & editing, Supervision, Formal analysis. **David C. Harrowven:** Writing – review & editing, Validation, Supervision, Resources, Project administration, Funding acquisition, Formal analysis, Conceptualization. **Steve P. Beeby:** Writing – review & editing, Validation, Supervision, Resources, Project administration, Funding acquisition, Formal analysis, Conceptualization.

Declaration of competing interest

The authors declare that they have no known competing financial interests or personal relationships that could have appeared to influence the work reported in this paper.

Data availability

All data supporting this study are openly available from the University of Southampton repository at https://doi.org/10.5258/SOTON/D2944.

Acknowledgement

The authors would like to thank the Engineering and Physical Sciences Research Council (EPSRC) for funding EP/S005307/1 (Functional electronic textiles for light emitting and colour changing applications) and EP/K039466/1 (Core Capability for Chemistry Research in Southampton), and European Regional Development Fund (ERDF) for funding InterReg V project 208 (SmartT: Smart Textiles for Regional Industry and Smart Specialisation Sectors). The work of Steve Beeby was supported by the Royal Academy of Engineering under the Chairs in Emerging Technologies Scheme (CiET2021\89).

References

[1] Y.H. Hwang, et al., Organic light-emitting fibers and fabrics for truly wearable smart displays: recent progress and future opportunities, J. Soc. Inf. Disp. 30 (10) (2022) 727–747.
[2] D. Janczak, et al., Stretchable and washable electroluminescent display screen-printed on textile, Nanomaterials 9 (9) (2019) 1276.
[3] A. Martin, A. Fontecchio, Effect of fabric integration on the physical and optical performance of electroluminescent fibers for lighted textile applications, Fibers 6 (3) (2018) 50.
[4] B. Hu, et al., Textile-based flexible electroluminescent devices, Adv. Funct. Mater. 21 (2) (2011) 305–311.
[5] M. de Vos, R. Torah, J. Tudor, Dispenser printed electroluminescent lamps on textiles for smart fabric applications, Smart Mater. Struct. 25 (4) (2016) 045016.
[6] S.B. Meier, et al., Light-emitting electrochemical cells: recent progress and future prospects, Mater. Today 17 (5) (2014) 217–223.
[7] K. Schlingman, et al., 25 Years of light-emitting electrochemical cells: a flexible and stretchable perspective, Adv. Mater. 33 (21) (2021) 2006863.
[8] Q. Pei, et al., Polymer light-emitting electrochemical cells, Science 269 (5227) (1995) 1086–1088.
[9] K. Youssef, et al., Fundamentals of materials selection for light-emitting electrochemical cells, Adv. Funct. Mater. 30 (33) (2020) 1909102.
[10] Y. Choe, et al., Small molecule-based light-emitting electrochemical cells, in: R. D. Costa (Ed.), Light-Emitting Electrochemical Cells: Concepts, Advances and Challenges, Springer International Publishing, Cham, 2017, pp. 329–349.
[11] T. Lanz, et al., A light–emission textile device: conformal spray-sintering of a woven fabric electrode, Flexible and Printed Electronics 1 (2) (2016) 025004.
[12] A. Sandström, et al., Ambient fabrication of flexible and large-area organic light-emitting devices using slot-die coating, Nat. Commun. 3 (1) (2012) 1002.
[13] S. Tang, L. Edman, Light-emitting electrochemical cells: a review on recent progress, Top. Curr. Chem. 374 (4) (2016) 40.
[14] S. Arumugam, et al., Spray-coated organic light-emitting electrochemical cells realized on a standard woven polyester cotton textile, IEEE Trans. Electron. Dev. 68 (4) (2021) 1717–1722.
[15] E. Auroux, et al., Solution-based fabrication of the top electrode in light-emitting electrochemical cells, Org. Electron. 84 (2020) 105812.
[16] S. Hu, J. Gao, 22 - materials and physics of light-emitting electrochemical cells (LECs), in: O. Ostroverkhova (Ed.), Handbook of Organic Materials for Electronic and Photonic Devices, second ed., Woodhead Publishing, 2019, pp. 727–757.
[17] M.Y. Wong, et al., Light-emitting electrochemical cells and solution-processed organic light-emitting diodes using small molecule organic thermally activated delayed fluorescence emitters, Chem. Mater. 27 (19) (2015) 6535–6542.
[18] S. Kanagaraj, A. Puthanveedu, Y. Choe, Small molecules in light-emitting electrochemical cells: promising light-emitting materials, Adv. Funct. Mater. 30 (33) (2020) 1907126.
[19] S. Arumugam, et al., Visible and ultraviolet light emitting electrochemical cells realised on woven textiles, Proceedings 68 (1) (2021) 9.
[20] H.-F. Chen, et al., UV light-emitting electrochemical cells based on an ionic 2,2′-bifluorene derivative, Org. Electron. 13 (10) (2012) 1765–1773.
[21] B. Liu, et al., Effect of chromophore-charge distance on the energy transfer properties of water-soluble conjugated oligomers, J. Am. Chem. Soc. 125 (2003) 6705. Arumugam, S., et al., Printable biflourene based ultra-violet (UV) organic light-emitting electrochemical cells (OLECs) with improved device performance. Organic Electronics, 2022. 105: p. 106513.
[22] L. Zhu, et al., Functionalization of poly(2,6-dimethyl-1,4-phenylene oxide)s with hindered fluorene side chains for anion exchange membranes, Macromolecules 49 (9) (2016) 3300–3309.